

Article

The Influence of Homogenous Magnetic Field Intensity on Surface Properties of Ni Thin Films Deposited from Citrate Baths and Their Role in Hydrogen Production

Safya Elsharkawy ^{1,2,*} , Dawid Kutyla ¹  and Piotr Żabiński ^{1,*} 

¹ Faculty of Non-Ferrous-Metals, AGH University of Krakow, Al. Mickiewicza 30, 30-059 Krakow, Poland; kutyla@agh.edu.pl

² Chemistry Department, Faculty of Science, Tanta University, Tanta 31527, Egypt

* Correspondence: elsharka@agh.edu.pl (S.E.); zabinski@agh.edu.pl (P.Ż.)

Abstract: Magnetic fields influence the deposition process and its current efficiency. They have a remarkable influence on thin films' surface characteristics and catalytic properties. Here, we study the correlation between the magnetic flux density and the current efficiency of the deposition process in the presence of a magnetic field with different intensities in different directions: the directions parallel and perpendicular to the electrode surface. We also show how the magnetic field direction impacts the surface roughness. Furthermore, we also analyze the impact of these synthesized films on the hydrogen evolution reaction (HER) when using them as electrocatalysts and how the application of a magnetic field in two dissimilar orientations influences the surface roughness and wettability. The synthesized Ni films are characterized using a scanning electron microscope (SEM), X-ray diffraction (XRD), and atomic force microscopy (AFM).

Keywords: magnetic field; electrodeposition; Ni films; hydrogen evolution reaction; citrate electrolyte



Citation: Elsharkawy, S.; Kutyla, D.; Żabiński, P. The Influence of Homogenous Magnetic Field Intensity on Surface Properties of Ni Thin Films Deposited from Citrate Baths and Their Role in Hydrogen Production. *Coatings* **2024**, *14*, 1459. <https://doi.org/10.3390/coatings14111459>

Academic Editor: Torsten Brezesinski

Received: 26 July 2024

Revised: 28 October 2024

Accepted: 5 November 2024

Published: 16 November 2024



Copyright: © 2024 by the authors. Licensee MDPI, Basel, Switzerland. This article is an open access article distributed under the terms and conditions of the Creative Commons Attribution (CC BY) license (<https://creativecommons.org/licenses/by/4.0/>).

1. Introduction

Nickel electroplating has garnered significant attention because of its industrial applications for both decorative and protective purposes. Electroplating stands out as a favored method due to its simplicity, cost-effectiveness, and applicability at low temperatures at the commercial scale [1,2]. The electrodeposition of Ni films from aqueous electrolytes has been extensively studied, utilizing different types of electrolytes including sulphamate, acetate, chloride, sulfate, lactate, and others. For instance, the Watts bath is considered predominant in the literature and commercial applications. This bath, containing nickel salts and boric acid along with additives, serves to regulate grain growth, which minimizes internal stresses and defines the coating properties [3,4]. An alternative approach involves using polycarboxylic acid salts, particularly citrates, in galvanic baths for nickel coating manufacture. These compounds, commonly employed in the electrodeposition of Ni-based alloys, offer a simpler chemical composition without surfactants [5–7]. Surprisingly, the fabrication of Ni coatings from citrate baths has received little attention.

Citrates act as complexing and buffering agents, facilitating the decomposition of heteropolymolybdate species and stabilizing the electrolyte pH. This contributes to the formation of homogeneous coatings with enhanced hardness, wear, and corrosion resistance. The initial findings suggest that nickel coatings obtained from citrate baths exhibit significantly higher hardness compared to those from Watts solutions. Sodium citrate, in particular, enhances the buffering capacity of an electrolyte solution, maintaining a high cathodic current efficiency and potentially influencing the grain size [8,9]. Despite these promising results, there remains a gap in well-ordered experimental research concerning the theoretical features of electrodeposition mechanisms. Further exploration is needed, particularly regarding the influence of the plating bath composition under neutral

to weakly alkaline pH conditions. Electrolysis parameters allow for the development of distinct microstructures and coating characteristics. The current efficiency is considered to be one of the most important parameters that can affect the deposition process. The properties of deposits have been studied in different articles [10–15].

When a magnetic field is introduced to an electrolyte, charged ions in the electrolytic cell undergo the Lorentz force, oriented perpendicularly to both the current density and the magnetic field. This force triggers convective motions in the electrolyte, leading to a reduction in the diffusion layer thickness. This phenomenon is known as the magnetohydrodynamic (MHD) effect [12].

Accordingly, this effect results in a rise in the limiting current density, which is denoted as j_L . The literature reports a linear correlation between j_L and $B^{1/3}$ (with B representing the magnetic flux density) for macroscopic electrodes [16,17], while microelectrodes exhibit a consistent correlation between j_L and B [18]. In addition to the Lorentz force, other forces may arise from variations in the magnetic field. These variations can be induced by the exterior magnetic field or by gradients in the concentration of paramagnetic ions (such as Cu^{2+} , Fe^{2+} , Co^{2+} , Ni^{2+} , etc.) [19,20]. The strength of the forces is contingent upon the dimensions of the magnetic field.

Coe et al. argue that the magnetic powers in an electrochemical reaction are six orders weaker than other forces such as diffusion and migration [21]. They conclude that the impact of magnetic forces becomes noteworthy only when merged with convective motions in an electrolyte. The process of nickel electrodeposition from water solutions typically involves the concurrent occurrence of the hydrogen evolution reaction (HER). As a result, the actual mass deposited over time is expected to be less than what is predicted by the Faraday law (Equation (1)) due to this accompanying reaction.

$$(dm/dt)_{calc} = MjA/nF \quad (1)$$

Here, M represents the molar mass of the deposited substance, j represents for current density, n denotes the number of electrons, F is the Faraday constant, and A is the surface area. Then, the current efficiency can be calculated using the ratio between the practical yield of the molar mass and the one calculated using the Faraday law. Chiba et al. [22] found that the current efficiency increased by 5 to 10% at $50 \pm 2^\circ\text{C}$ when a magnetic field up to 0.15 T was present (aligned with the electric field).

Conversely, Devos et al. [23] noted a reduction of a few percentage points when applying a magnetic field of 1 T in the perpendicular direction of the electric field [24]. A numerical analysis was conducted by Shannon et al. on the relationship between the roughness of the fabricated surface and the direction of the magnetic field. It was noticed that applying the magnetic field in a parallel orientation to the electric field raised the roughness value compared to the value obtained for the perpendicular direction.

Danilyuk asserted that for copper, specific magnetic field values (ranging from 60 to 160 mT) expedite the electrodeposition behavior, while others (from 160 to 173 mT) hinder it. For nickel and tin, these regions alternate.

Consequently, alterations in structure and morphology may occur [25]. Considering the diverse effects of a magnetic field on an electrochemical reaction, there is potential to customize magnetic intensities to enhance mass transport or the characteristics of the fabricated layer.

Nevertheless, a more thorough comprehension of the fundamental interactivity between magnetic fields and electrochemical reactions is essential before effective customization occurs. Regarding the energy crisis, the world must find a renewable and green energy source. The hydrogen evolution reaction (HER) has recently gained attention because of the potential use of H_2 as a green fuel. Many studies have been carried out to understand the mechanism of this reaction [26,27]. The properties of the catalyst are determined by the metal/metal oxide interface where the adsorption of hydrogen intermediates occurs.

The metal oxide exhibits hydrophilic properties that facilitate the sorption of hydroxyl ions [28]. The electrodeposition of metals allows for the fabrication of cathodes suitable for

use in water-splitting reactions as alternatives to noble metals [29,30]. To date, Pt and Ru electrocatalysts have been used for hydrogen evolution reactions. However, the scarcity of their use refers to their rarity and high price. As a result, scientists are trying to design an efficient electrocatalyst with great abundance and economical price.

Ni is one of the most promising electrocatalysts for water-splitting reactions [15,31–36]. Ni cones, which are produced through a single electrodeposition method, can serve as catalysts for the hydrogen evolution reaction (HER) due to the heightened active surface area [37]. Additionally, these cones are recognized for their superhydrophobic characteristics [38]. Furthermore, the catalytic performance of Ni cones can be enhanced by modifying them with noble metals [37].

Most catalysts employed in water splitting are typically in powder form and necessitate a binder or gluey agent, for instance, Nafion, for attachment to the electrode surface. However, using these binders can obstruct the catalyst's active sites over time, reducing the stability and the catalytic activity. Fuzhan et al. developed a unique Ni₃N/Ni electrocatalyst through interface engineering, exhibiting excellent hydrogen evolution and oxidation activities in aqueous electrolytes.

The electrocatalyst demonstrated nearly zero overpotential in an alkaline solution and required only 12 mV to attain a current density of 10 mA cm⁻² in a neutral solution [39]. Huimin Wang synthesized a CeO_x-NiB@NF electrode, producing a 19 mV overpotential to achieve a current density value of 10 mA cm⁻² for the HER [40]. Tharanga N produced Ni_{2-x}Rh_xP nanoparticles requiring 200 mV overpotential to achieve a current density of 10 mA cm⁻² in 0.5 M H₂SO₄ [41].

Ping Qin et al. [42] have synthesized a honeycomb Ni₃N-Co₃N on carbon cloth to investigate the direct oxygen evolution reaction mechanism. It produced overpotential values of 320 and 495 mV to achieve a current density of 10 and 100 mA cm⁻², respectively. Katarzyna Skibińska et al. synthesized Ni-Cu alloy using an electrodeposition method with one simple step using the magnetic field for hydrogen production [43]. El-hallag et al. fabricated Ni nanoparticles at a pencil graphite electrode (PGE) from deep eutectic solvent and studied the influence of the deposition parameters for hydrogen production [32].

Zining and colleagues fabricated 3D nanosheet arrays of NiMoO₄ on nickel foam with Iron-doped carbon quantum dots (Fe-CQDs/NiMoO₄/NF), resulting in an overpotential of 117 mV to achieve a current density of 10 mA cm⁻² in alkaline conditions [44]. To address this issue, the electrodeposition technique emerges as a crucial and cost-effective method for preparing nanomaterials, facilitating the creation of highly active catalysts.

This article aims to prepare fabricated Ni films from citrate solution under the impact of the magnetic field in different directions and with different magnetic flux densities. The second aim was to study the relationship between the magnetic field intensity and the current efficiency. Additionally, we studied the effect of these different intensities on the surface morphologies of the deposits and surface wettability, and hence how this impacts their catalytic performance in the HER.

2. Experiments

2.1. Materials and Methods

The electrolyte solution was composed of citric acid with a concentration of 0.2 M and sodium citrate with a concentration of 0.2 M. Both nickel chloride and nickel sulfate were put into the electrolyte and the pH was modified to 1.47. In our previous studies [31,45], we prepared Ni films from three solutions and studied the optimization process. We have chosen the optimum conditions for the best electrolyte and the best pH to work with this article.

2.2. Synthesis of Ni Films

The electrochemical deposition was conducted using a three-electrode configuration cell. A working electrode (WE) made of Cu with a surface area of 2.82 cm² and a counter electrode (CE) made of platinum mesh were utilized, with a saturated calomel electrode as

the reference (RE). In order to prevent interference from the back and side faces, the working electrode was mounted on a Teflon holder. Before each deposition cycle, the working electrode underwent chemical treatment in a solution with concentrated HNO_3 , H_3PO_4 , and CH_3COOH (in a 1:1:1 volume ratio) at 85°C for 15 s. The deposition process utilized a chronoamperometric technique employing a Bio-Logic SAS Model SP-200 potentiostat. An electromagnet (Lake Shore Model 642, Lake Shore Cryotronics, Inc., Westerville, OH, USA) was employed to create a uniform external magnetic field. This magnetic field is oriented perpendicularly (B_{\perp} , along the x-direction) and parallel (B_{\parallel} , along the -y-direction) to the electrodes, with strengths ranging from 0.1 T to 0.5 T. The electrodeposition process has been performed by using the chronoamperometry technique at a specific potential value of -1.2 V for 10 min. Because the fabricated Ni material displayed ferromagnetism, it became magnetized by the external field, leading to localized magnetic field effects near the electrode surface. Alongside the Lorentz force resulting from potential surface changes, the magnetic gradient force could induce electrolyte flows nearby, affecting mass transfer.

2.3. Electrochemical Investigations of Hydrogen Evolution Reaction (HER)

The fabricated Ni coatings were evaluated in a traditional three-electrode system. The freshly prepared electrocatalysts were employed as the working electrode, while a saturated calomel electrode (SCE) and a Pt wire acted as the reference and counter electrodes, respectively. Linear sweep voltammetry (LSV) analyses have been performed relative to the saturated calomel electrode, using a scan rate of 5 mV s^{-1} in a solution comprising 1 M NaOH.

2.4. Characterization of Ni Films

JEOL-JCM-6000 PLUS Scanning Electron Microscope (SEM) from Tokyo, Japan, has been employed to analyze the surface morphology of the deposited thin films. X-ray diffraction (XRD) was also conducted using a Rigaku MiniFlex II instrument from Tokyo, Japan, to show the crystalline structure of the deposits. Atomic force microscopy (AFM) NTegra Aura NT MDT (Moscow, Russia) in a semicontact mode using an NSG03 tip was used to perform the 3-D topography images of the deposits. Wettability measurements were carried out using a Fast Camera Model: 9501 with HiBestViewer 1.0.5.1 Software from San Diego, CA, USA, Photron company. Distilled water has been used for measuring the contact angle by putting a $10\ \mu\text{L}$ droplet on the fabricated surface. The contact angle was calculated using ImageJ Software version 2 (GPLv2).

3. Results and Discussion

3.1. The Impact of the Magnetic Field Intensity on Nickel Coating Morphologies

Figure 1a–i show the SEM images of the deposited Ni thin films in the presence and absence of the magnetic field with different intensities. Figure 1a represents the SEM images of thin films prepared without the application of B and (b–e) in the existence of B_{\perp} in the presence of different B_{flux} densities (0.1, 0.2, 0.3, and 0.5 T, respectively). Figure 1f–i show the SEM images for the fabricated films in the presence of different B_{flux} densities (0.1, 0.2, 0.3, and 0.5 T, respectively). It is evident that in the absence of B , the surface has a lot of voids and holes which are indicated by the marked red circles in the case of the B_{flux} density ranging from 0.1 T to 0.3 T, while at the highest B_{flux} density value of 0.5 T, the number of voids and holes is decreased and the formation of spherical particles is observed. In the case of applying B in two different directions, B_{\perp} and B_{\parallel} , with various intensities from 0.1 T to 0.3 T, the surface did not have many differences in both directions but the number of voids and the number of holes started to decrease compared to without using the magnetic field and the surface became smoother. The number of holes decreased more when using a high magnetic field density of 0.5 T in both directions and the surface became even smoother with small spherical particles.

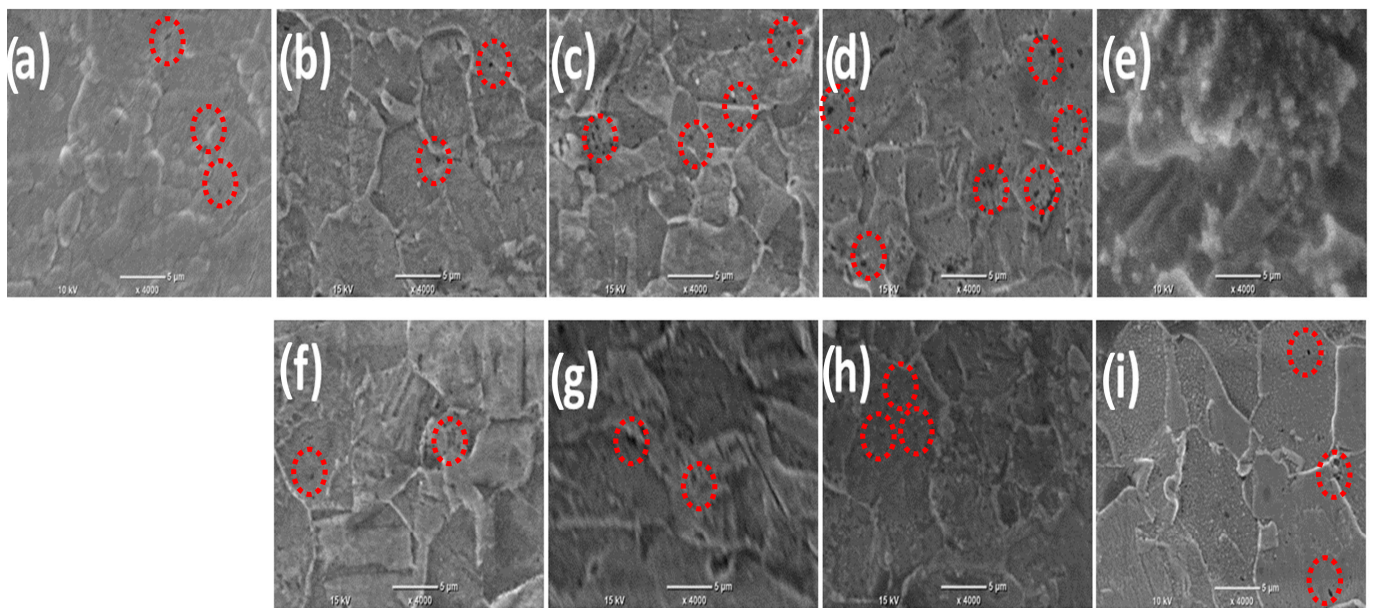


Figure 1. SEM images of Ni deposits without B (a), existence of B_{\perp} (b–e), (f–i) presence of B_{\parallel} with different intensities ranging from (0.1–0.5 T), respectively. The red circles represent the holes appear in the surface.

3.2. XRD Analysis

Figure 2 represents the XRD pattern of the Ni coatings deposited from the citrate solution at a potential value of -1.2 V and pH 1.47 in the presence of B in the directions parallel and perpendicular to the electrode surface. Two diffraction peaks appear for the Cu substrate at 2θ values of 43.4° and 50.68° , which relate to the diffraction planes (111) and (200), respectively, according to JCDPS card no. 00-001-1242. Furthermore, no diffraction peaks appear for the deposited Ni in both directions. This refers to the thickness of the fabricated Ni film being too small while the high-intensity peak for the Cu substrate blocks the Ni peaks from being visible. The calculated thickness for the fabricated Ni in the presence of B_{\parallel} and B_{\perp} is $0.33\ \mu\text{m}$ and $0.17\ \mu\text{m}$ and $0.98\ \mu\text{m}$ for the Ni prepared in the absence of the B.

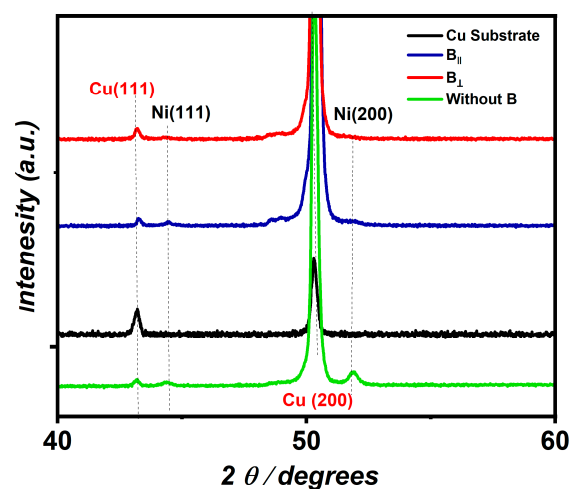


Figure 2. XRD spectrum of fabricated Ni (JCDPS card no. 00-001-1242) in the presence of B_{\parallel} and B_{\perp} . Figure 2 is reproduced according to our data, which are published in ref. [39].

3.3. The Influence of the Magnetic Field Intensity on the Current Efficiency of the Electrodeposition Process

Figure 3 exhibits the relationship between the current efficiency and the magnetic flux density (B). The current efficiency was calculated for the Ni deposits of B_{\perp} and B_{\parallel} at different intensities. It was found that with increasing intensity up to 0.2 T, the current efficiency rises, and by increasing the intensity value up to 0.5 T, the current efficiency decreases. However, the current efficiency for the electrodeposition in the B_{\perp} direction was found to be higher than the current efficiency obtained for the deposition process in the B_{\parallel} direction. The overall current density comprises the reduction in the Ni ion current and the evolved hydrogen gas (HER). The evolved hydrogen gas during the deposition of metals from aqueous solutions holds particular significance in electrochemical reactions [43,44]. This interest stems partly from concerns about hydrogen embrittlement, which can adversely affect the mechanical properties of metals. In a magnetic field, magnetohydrodynamic stirring generates an elevation in both limiting current densities. The extent of this increase is contingent upon various factors, including the magnetic flux density and concentration [44]. Given the significantly higher concentration of nickel ions compared to protons, it can be inferred that B has a more pronounced effect on nickel deposition. Therefore, hydrogen evolution proceeds easily in the absence of B and then it consumes current for the HER, and not for the deposition, so the current efficiency decreases.

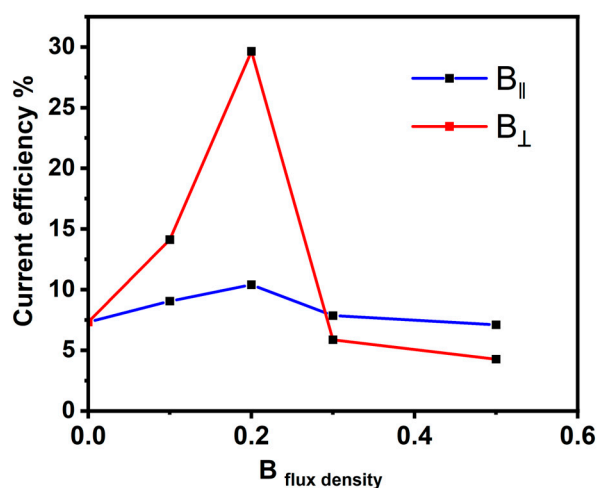


Figure 3. Current efficiency and magnetic flux density are related in both parallel and perpendicular directions.

3.4. The Effect of the Magnetic Flux Density on the Surface Wettability

Figure 4 exhibit the impact of the $B_{\text{flux density}}$ on the surface wettability. We have studied the impact of B in the vertical and horizontal directions, respectively, during the deposition process with different intensities ranging from 0.1 to 0.5 T. It has been elucidated that the prepared nickel deposits from both directions at different magnetic flux densities have hydrophilic properties and contact angles less than 90 degrees. However, there is a remarkable relationship: as the magnetic flux density increases, the contact angles value increases. Furthermore, increasing the contact angles of the surface increases the catalytic performance of the HER, which has been proven in the linear sweep voltammetry (LSV) experiment for testing the performance of the HER. This refers to the tendency of the surface to be less hydrophilic as the catalytic effect on the HER increases as the residual time for the hydrogen and oxygen bubbles on the surface decreases, and hence, this will provide more active sites for the reaction.

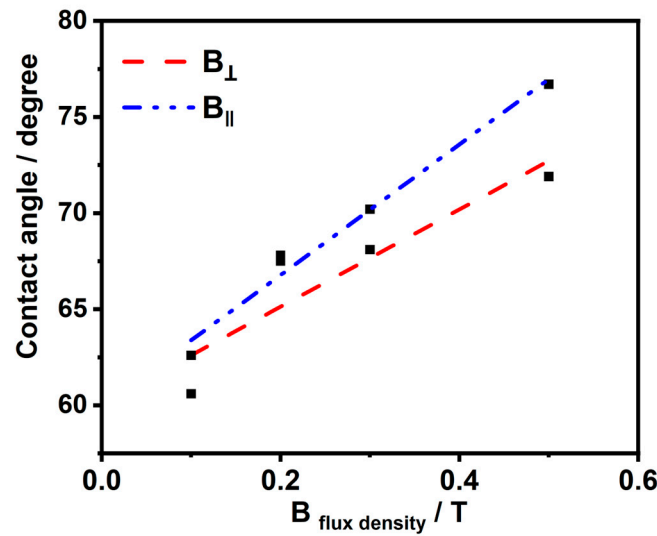


Figure 4. Contact angle–magnetic field flux density correlation.

3.5. The Influence of Magnetic Field Direction on the Roughness of the Deposits

Figure 5a–c exhibit the AFM 3D image measurements of the nickel coatings from citrate at pH 1.47 at a deposition potential of -1.2 V in the absence and existence of the magnetic field in both the horizontal and vertical directions at 0.5 T, respectively. It is noticeable that AFM images exhibit some holes and grains. Additionally, the presence of a significant alteration in the roughness value of the deposited nickel coatings with and without B in two different directions is remarkable. Moreover, the area of the nickel coatings from citrate in the presence of B_{\perp} shows the smoothest and flattest surface, as indicated in Figure 5c.

The roughness values were measured for all the deposited nickel samples. The roughness of the fabricated Ni in the presence of B_{\perp} has a value of 29 nm, which is the lowest roughness value obtained compared to the fabricated Ni in the presence of B_{\parallel} and in the absence of B, which has a value of 101 nm and 141 nm, respectively. In general, the formation of surface roughness results from uneven nucleation and crystal growth, contributing to the overall texture [42]. The results show that the magnetic field influences the roughness of the surface and reduces the roughness value. Moreover, the direction has a significant impact on this roughness value as it has been found that applying a magnetic field in the perpendicular orientation decreases the roughness and makes the surface smoother compared to the magnetic field applied in the horizontal direction. Table 1 contains the different values of the roughness measurements for the Ni deposits in both the B_{\parallel} and B_{\perp} directions to the electrode surface.

Table 1. Roughness values for fabricated Ni in presence of B_{\parallel} and B_{\perp} .

Ni Films	Roughness (nm)
Absence of B	141
B_{\perp}	29
B_{\parallel}	101

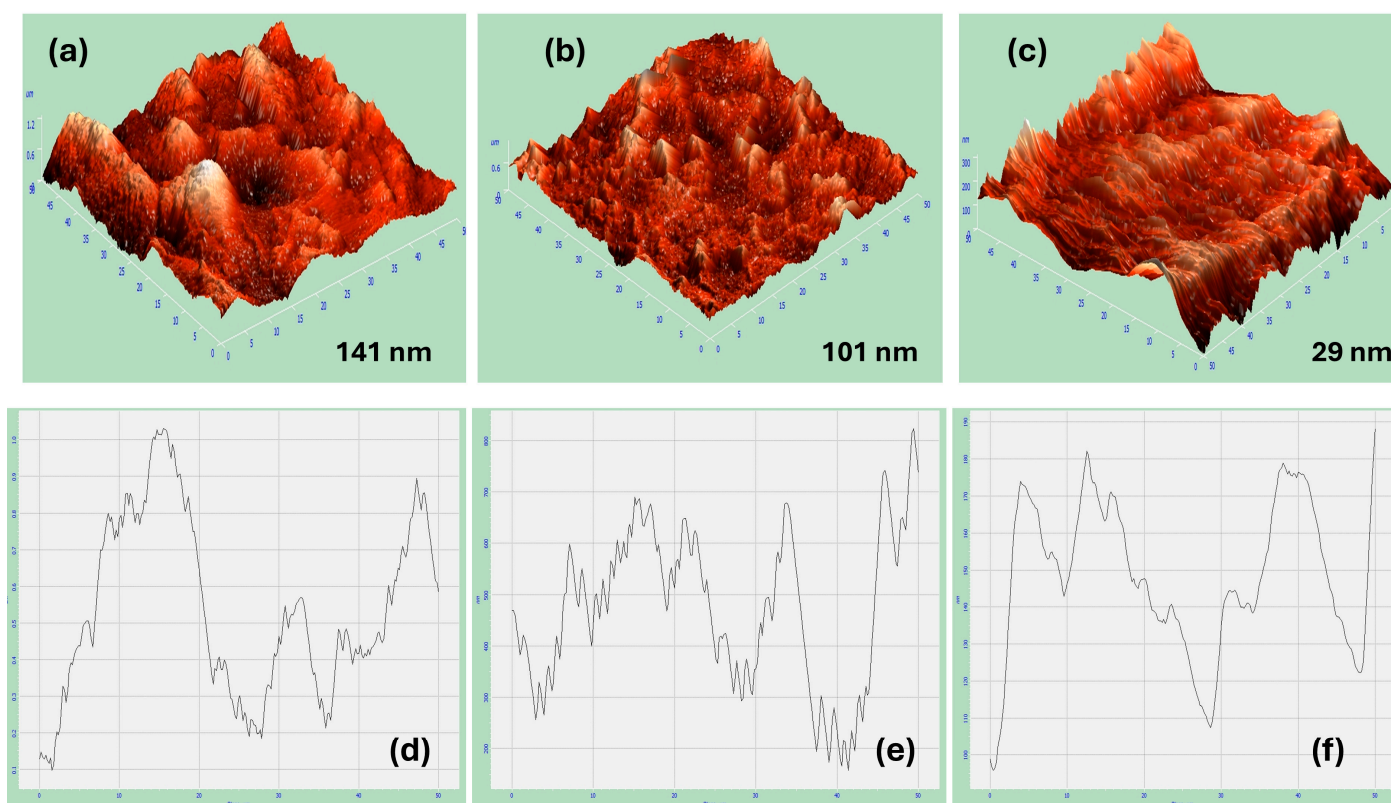


Figure 5. AFM 3D images for (a) fabricated Ni thin films in absence of B , (b) in presence of B_{\parallel} , (c) and in presence of B_{\perp} . (d–f) are their line scans, respectively.

3.6. The Impact of Magnetic Flux Density on the Electrocatalytic Activity of Nickel Coatings Synthesized by the Effect of the Magnetic Field in Perpendicular Direction on the HER and Its Correlation with the Contact Angle

Figure 6a,b represent the cathodic polarization curves for 1 M NaOH at a scan rate value of 5 mV s^{-1} for the Ni deposits from citrate in the presence of B_{\perp} with different $B_{\text{flux densities}}$ ranging from 0.1 T to 0.5 T and their Tafel slopes, respectively. It has been found that the overpotential values (η) obtained for the Ni thin films under flux densities from 0.1 T to 0.3 T have no significant change and have a nearly identical value of -297 mV , achieving a current density value of 10 mA cm^{-2} . However, by increasing the magnetic flux density to a higher value of 0.5 T, the overpotential for the HER is found to be -240 mV , attaining a current density value of 10 mA cm^{-2} , which has the smallest result compared to that of the others. Therefore, with the enlargement of the magnetic field intensity, this produces a more consistent and smooth surface with the highest catalytic activity in the HER. Further, the Tafel slopes were found to have the smallest value referring to the Ni thin film prepared at high magnetic field flux density, while the highest value related to the Ni thin film was synthesized at a low magnetic flux density. This shows that the Ni film fabricated at a high magnetic flux density possesses the highest catalytic performance in the HER.

Moreover, we have measured the contact angles of the fabricated deposits. It has been found that with the rising magnetic field intensity, the contact angle increases, which means that the highest contact angle refers to the fabricated Ni with a magnetic flux density of 0.5 T and the smallest value belongs to the fabricated Ni at the lowest magnetic flux density of 0.1 T. The increase in the catalytic performance for the hydrogen evolution reaction (HER) is associated with a decrease in surface hydrophilicity. This is due to the increased availability of free space on the surface, resulting in a shorter residual time for hydrogen and a higher number of active sites on the electrode surface. The nickel deposits produced from citrate at a high magnetic flux density (0.5 T) exhibited a significantly higher exchange

current density (j_0) of $20 \times 10^{-1} \text{ A cm}^{-2}$ compared to that of the nickel layers fabricated at lower magnetic flux densities ($1 \times 10^{-1} \text{ A cm}^{-2}$, $4.9 \times 10^{-2} \text{ A cm}^{-2}$, $4.6 \times 10^{-1} \text{ A cm}^{-2}$ for each fabricated film with magnetic field flux densities of 0.1 T, 0.2 T, and 0.3 T, respectively). Table 2 provides information on the overpotential, Tafel slopes, contact angles, and kinetics studies for each Ni film synthesized at different magnetic flux densities. The kinetics variables (j_0 and α) were determined using Tafel Equations (3)–(5) [31].

$$\eta = a + b \log j \quad (2)$$

$$a = \frac{2.3RT}{\alpha nF} \log j_0 \quad (3)$$

$$b = \frac{-2.3RT}{\alpha nF} \quad (4)$$

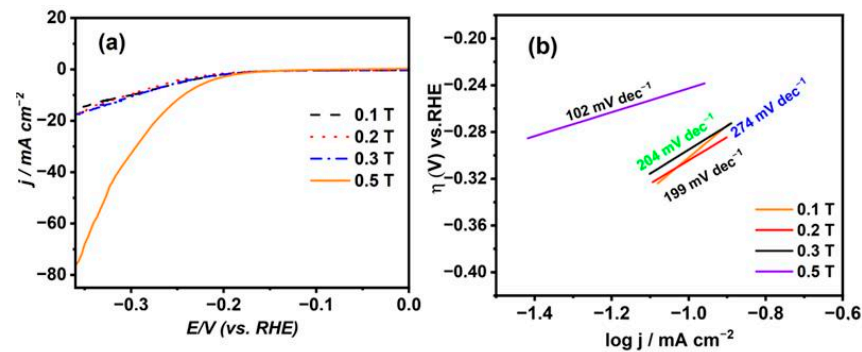


Figure 6. (a) LSV for 1 M NaOH at nickel layers deposited from citrate electrolyte under the influence of B_{\perp} with different magnetic flux densities and (b) their Tafel plots.

Table 2. Values of overpotential, Tafel slopes, and contact angles values for HER of synthesized Ni electrodes at different magnetic flux densities.

Ni Thin Film at Different Magnetic Flux Densities	η_{10} (mV)	Tafel Slope (mV dec ⁻¹)	Contact Angle	j_0 (A cm ⁻²)	α
0.1 T	-295	274	61	1×10^{-1}	0.09
0.2 T	-296	199	68	4.9×10^{-1}	0.135
0.3 T	-297	204	68.4	4.6×10^{-1}	0.132
0.5 T	-240	102	72	20×10^{-1}	0.2

The expression η represents the applied overpotential for the hydrogen evolution reaction (HER), with a denoting the intercept, b as the Tafel slope, j representing the cathodic current density, R as the gas constant, T as the absolute temperature, n as the number of exchanging electrons, F as Faraday's constant, α as the charge transfer coefficient, and j_0 as the exchange current density. Plotting the overpotential (η) on the y -axis and $\log j$ on the x -axis produces a straight line characterized by slope (b) and intercept (a), which are utilized to determine the kinetics parameters of j_0 and α for the HER at the Ni electrodes formed through electrodeposition. According to the details in Table 2, the nickel coatings produced using citrate solution and the highest magnetic flux density exhibit the highest j_0 value, indicating superior catalytic activity compared to that of the other electrodes. Moreover, it demonstrates an elevated α value of 0.20, signifying improved catalytic productiveness in the HER. Additionally, it features the smallest Tafel slope, recorded at 102 mV dec^{-1} , suggesting a predominant Volmer–Heyrovsky reaction mechanism for the reaction [32].

3.7. Durability and Stability Studies

Figure 7 provides the cathodic polarization curves for 1 M NaOH at a scan rate of 5 mV s^{-1} for the nickel coatings synthesized from the citrate electrolyte in the presence of B_{\perp} at the highest magnetic flux density of 0.5 T. It has been noticed that the overpotential has slightly changed from a value of 274 mV after 1 cycle to be 286 mV after 1000 cycles to reach a current density of 10 mA cm^{-2} . This shows that the Ni film has a high durability for the HER. Moreover, Figure 7b shows that the stability measurement for the deposited nickel coatings have been accomplished utilizing the chronoamperometry technique at -1.3 V vs. SCE for 24 h. It is remarkable that the synthesized Ni electrode produces a high current density, proving it contains more active sites. Moreover, the current density after 1584 s is -2.31 mA cm^{-2} . Additionally, after 10,801 s, the current retention became 68%. This shows that the Ni coatings prepared from citrate at a high magnetic flux density have a higher current density, proving their high mechanical stability for the HER.

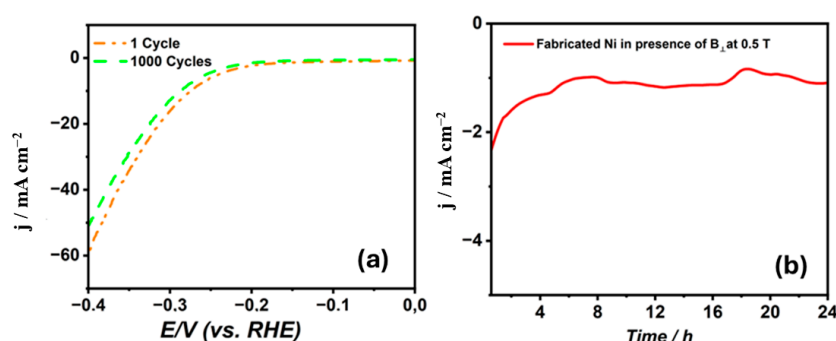


Figure 7. (a) Cathodic polarization curves for 1 M NaOH at 5 mV s^{-1} after 1 and 1000 cycles. (b) Chronoamperometric stability curve over 24 h.

Furthermore, SEM images were captured of the prepared nickel coatings after the stability test to assess the potential changes in the morphology. In Figure 8a,b, the SEM images depict the Ni film deposited from citrate under the magnetic field's effect at 0.5 T perpendicular to the electrode surface, both before and after the stability test. The images reveal that the surface morphology slightly changes but shows no significant alterations, indicating excellent stability as an electrocatalyst.

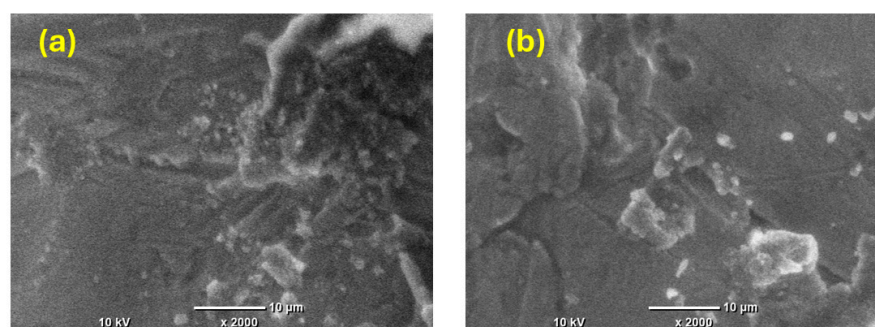


Figure 8. SEM images of Ni film fabricated from citrate under the influence of B_{\perp} at 0.5 T (a) before the stability measurement and (b) after the stability measurement.

4. Conclusions

The magnetic flux density significantly influences the morphology of deposits from citrate electrolytes, altering their surface properties. As the magnetic field intensity increases in both the parallel and perpendicular directions, there are notable changes in the current efficiency of the deposition reaction.

Additionally, the magnetic flux density affects the wettability of the fabricated nickel (Ni) surface. As the magnetic field density increases, the contact angle of the Ni surface

also increases. This wettability change impacts the Ni deposits' catalytic effectiveness for hydrogen evolution reactions (HERs). The magnetic field direction affects the morphology and hence the properties of the prepared film in the HER. The Ni film prepared under a magnetic field in the perpendicular direction shows higher catalytic activity compared to that of the film prepared in the parallel direction. Moreover, the direction of the magnetic field affects the roughness value for each prepared film, and produces a smaller value for the film obtained in the perpendicular direction.

Among the various magnetic field intensities studied, the highest intensity of 0.5 Tesla (T) produces a Ni thin film with the lowest overpotential value for the HER, making it more efficient compared to Ni films fabricated at lower magnetic field flux densities.

Author Contributions: Conceptualization, S.E.; performing the experiments and writing—original draft preparation, D.K.; writing—original draft preparation, P.Ż. All authors have read and agreed to the published version of the manuscript.

Funding: My article has been funded under project number 10572. The research project was supported by program "Excellence initiative-Research University" for the AGH University of Krakow.

Institutional Review Board Statement: Not applicable.

Informed Consent Statement: Not applicable.

Data Availability Statement: The raw/processed data required to reproduce these findings cannot be shared at this time as the data also form part of an ongoing study.

Conflicts of Interest: The authors declare no conflicts of interest.

References

1. Pogrebnjak, A.D.; Novosad, V. Advances in Thin Films, Nanostructured Materials, and Coatings. In *Lecture Notes in Mechanical Engineering, Proceedings of the 2018 International Conference on "Nanomaterials: Applications & Properties, Odesa, Ukraine, 28–30 December 2018*; Springer Nature Singapore: Singapore, 2019; ISBN 9789811361326.
2. Xizhang, C.; Su, C.; Wang, Y.; Siddiquee, A.N.; Sergey, K.; Jayalakshmi, S.; Singh, R.A. Cold Metal Transfer (CMT) Based Wire and Arc Additive Manufacture (WAAM) System. *J. Synch. Investig.* **2018**, *12*, 1278–1284. [[CrossRef](#)]
3. Godon, A.; Creus, J.; Feaugas, X.; Conforto, E.; Pichon, L.; Armand, C.; Savall, C. Characterization of Electrodeposited Nickel Coatings from Sulphamate Electrolyte without Additive. *Mater. Charact.* **2011**, *62*, 164–173. [[CrossRef](#)]
4. Godon, A.; Creus, J.; Cohendoz, S.; Conforto, E.; Feaugas, X.; Girault, P.; Savall, C. Effects of Grain Orientation on the Hall–Petch Relationship in Electrodeposited Nickel with Nanocrystalline Grains. *Scr. Mater.* **2010**, *62*, 403–406. [[CrossRef](#)]
5. Lima-Neto, P.D.; Correia, A.N.; Vaz, G.L.; Casciano, P.N.S. Morphological, Structural, Microhardness and Corrosion Characterisations of Electrodeposited Ni-Mo and Cr Coatings. *J. Braz. Chem. Soc.* **2010**, *21*, 1968–1976. [[CrossRef](#)]
6. Beltowska-Lehman, E.; Bigos, A.; Indyka, P.; Kot, M. Electrodeposition and Characterisation of Nanocrystalline Ni–Mo Coatings. *Surf. Coat. Technol.* **2012**, *211*, 67–71. [[CrossRef](#)]
7. Halim, J.; Abdel-Karim, R.; El-Raghy, S.; Nabil, M.; Waheed, A. Electrodeposition and Characterization of Nanocrystalline Ni-Mo Catalysts for Hydrogen Production. *J. Nanomater.* **2012**, *2012*, 1–9. [[CrossRef](#)]
8. Doi, T.; Mizumoto, K.; Tanaka, S.; Yamashita, T. Bright Nickel Plating from Nickel Citrate Electroplating Baths. *Met. Finish.* **2004**, *102*, 26–35. [[CrossRef](#)]
9. Chaoqun, L.; Xinhai, L.; Zhixing, W.; Huajun, G. Mechanism of Nanocrystalline Nickel Electrodeposition from Novel Citrate Bath. *Rare Met. Mater. Eng.* **2015**, *44*, 1561–1567. [[CrossRef](#)]
10. Bund, A.; Ispas, A. Influence of a Static Magnetic Field on Nickel Electrodeposition Studied Using an Electrochemical Quartz Crystal Microbalance, Atomic Force Microscopy and Vibrating Sample Magnetometry. *J. Electroanal. Chem.* **2005**, *575*, 221–228. [[CrossRef](#)]
11. Feiler, A.A.; Davies, P.T.; Vincent, B. Adsorption of Anionic Gold Nanoparticles by a Layer of Cationic Microgel Particles Deposited on a Gold-Coated, Quartz Surface: Studied by Quartz Crystal Microbalance and Atomic Force Microscopy. *Soft Matter* **2011**, *7*, 6660. [[CrossRef](#)]
12. Chopart, J.P.; Douglade, J.; Fricoteaux, P.; Olivier, A. Electrodeposition and Electrodissolution of Copper with a Magnetic Field: Dynamic and Stationary Investigations. *Electrochim. Acta* **1991**, *36*, 459–463. [[CrossRef](#)]
13. Lee, J.; Ragsdale, S.R.; Gao, X.; White, H.S. Magnetic Field Control of the Potential Distribution and Current at Microdisk Electrodes. *J. Electroanal. Chem.* **1997**, *422*, 169–177. [[CrossRef](#)]
14. O'Brien, R.N.; Santhanam, K.S.V. Magnetic Field Assisted Convection in an Electrolyte of Nonuniform Magnetic Susceptibility. *J. Appl. Electrochem.* **1997**, *27*, 573–578. [[CrossRef](#)]

15. Waskaas, M.; Kharkats, Y.I. Magnetoconvection Phenomena: A Mechanism for Influence of Magnetic Fields on Electrochemical Processes. *J. Phys. Chem. B* **1999**, *103*, 4876–4883. [[CrossRef](#)]
16. Long, Q.; Zhong, Y.; Wu, J. Effect of Magnetic Fields on the Behavior of Iron Electrodeposition. *Int. J. Electrochem. Sci.* **2020**, *15*, 6955–6968. [[CrossRef](#)]
17. Chiba, A.; Hosokawa, A.; Ogawa, T. Inhibition of Dendrites of Tin from Tin (II) Sulphate- Sulphuric Acid by Magnetic Fields. *Surf. Coat. Technol.* **1986**, *27*, 131–136. [[CrossRef](#)]
18. Devos, O.; Olivier, A.; Chopart, J.P.; Aaboubi, O.; Maurin, G. Magnetic Field Effects on Nickel Electrodeposition. *J. Electrochem. Soc.* **1998**, *145*, 401–405. [[CrossRef](#)]
19. Chouchane, S.; Levesque, A.; Zabinski, P.; Rehamnia, R.; Chopart, J.-P. Electrochemical Corrosion Behavior in NaCl Medium of Zinc–Nickel Alloys Electrodeposited under Applied Magnetic Field. *J. Alloys Compd.* **2010**, *506*, 575–580. [[CrossRef](#)]
20. Danilyuk, A.L.; Kurmashev, V.I.; Matyushkov, A.L. Magnetostatic Field Influence on Electrodeposition on Metal Films. *Thin Solid. Film.* **1990**, *189*, 247–255. [[CrossRef](#)]
21. Lasia, A. Mechanism and Kinetics of the Hydrogen Evolution Reaction. *Int. J. Hydrog. Energy* **2019**, *44*, 19484–19518. [[CrossRef](#)]
22. Chen, L.; Lasia, A. A Study of the Kinetics of Hydrogen Evolution Reaction on Nickel-Zinc Alloy Electrodes. *J. Electrochem. Soc.* **1991**, *138*, 3321. [[CrossRef](#)]
23. Liang, Z.; Ahn, H.S.; Bard, A.J. A Study of the Mechanism of the Hydrogen Evolution Reaction on Nickel by Surface Interrogation Scanning Electrochemical Microscopy. *J. Am. Chem. Soc.* **2017**, *139*, 4854–4858. [[CrossRef](#)] [[PubMed](#)]
24. Kutyla, D.; Kołczyk-Siedlecka, K.; Kwiecińska, A.; Skibińska, K.; Kowalik, R.; Żabiński, P. Preparation and Characterization of Electrodeposited Ni-Ru Alloys: Morphological and Catalytic Study. *J. Solid. State Electrochem.* **2019**, *23*, 3089–3097. [[CrossRef](#)]
25. Zhang, K.; Liu, J.; Xiao, W.; Yan, C. Electrodeposition of Graded Ni-S Film for Hydrogen Evolution Reaction. *Mater. Lett.* **2017**, *193*, 77–80. [[CrossRef](#)]
26. Elsharkawy, S.; Kutyla, D.; Zabinski, P. The Influence of the Magnetic Field on Ni Thin Film Preparation by Electrodeposition Method and Its Electrocatalytic Activity towards Hydrogen Evolution Reaction. *Coatings* **2023**, *13*, 1816. [[CrossRef](#)]
27. El-Hallag, I.; Elsharkawy, S.; Hammad, S. The Effect of Electrodeposition Potential on Catalytic Properties of Ni Nanoparticles for Hydrogen Evolution Reaction (HER) in Alkaline Media. *J. Appl. Electrochem.* **2022**, *52*, 907–918. [[CrossRef](#)]
28. El-Esawy, M.A.; Elsharkawy, S.; Youssif, M.M.; Raafat Tartour, A.; Ramadan Elsharkawy, F.; Ahmed Saad Badr, S.; Elghoraby, A.M.; Elsayed Gad, M.; Etman, A.E.; Essam Mahmoud, F.; et al. Recent Advances of Green Nanoparticles in Energy and Biological Applications. *Mater. Today* **2023**, *72*, 117–139. [[CrossRef](#)]
29. Skibińska, K.; Elsharkawy, S.; Kula, A.; Kutyla, D.; Żabiński, P. Influence of Substrate Preparation on the Catalytic Activity of Conical Ni Catalysts. *Coatings* **2023**, *13*, 2067. [[CrossRef](#)]
30. Elsharkawy, S.; Hammad, S.; El-hallaga, I. Electrodeposition of Ni Nanoparticles from Deep Eutectic Solvent and Aqueous Solution Promoting High Stability Electrocatalyst for Hydrogen and Oxygen Evolution Reactions. *J. Solid. State Electrochem.* **2022**, *26*, 1501–1517. [[CrossRef](#)]
31. Kawondera, R.; Bonechi, M.; Maccioni, I.; Giurlani, W.; Salzillo, T.; Venuti, E.; Mishra, D.; Fontanesi, C.; Innocenti, M.; Mehlana, G.; et al. Chiral “Doped” MOFs: An Electrochemical and Theoretical Integrated Study. *Front. Chem.* **2023**, *11*, 1215619. [[CrossRef](#)]
32. Giurlani, W.; Fidi, A.; Anselmi, E.; Pizzetti, F.; Bonechi, M.; Carretti, E.; Lo Nostro, P.; Innocenti, M. Specific Ion Effects on Copper Electroplating. *Colloids Surf. B Biointerfaces* **2023**, *225*, 113287. [[CrossRef](#)] [[PubMed](#)]
33. Darband, G.B.; Aliofkhaezai, M.; Sabour Rouhaghdam, A. Nickel Nanocones as Efficient and Stable Catalyst for Electrochemical Hydrogen Evolution Reaction. *Int. J. Hydrog. Energy* **2017**, *42*, 14560–14565. [[CrossRef](#)]
34. Lee, J.M.; Jung, K.K.; Lee, S.H.; Ko, J.S. One-Step Fabrication of Nickel Nanocones by Electrodeposition Using $\text{CaCl}_2 \cdot 2\text{H}_2\text{O}$ as Capping Reagent. *Appl. Surf. Sci.* **2016**, *369*, 163–169. [[CrossRef](#)]
35. Song, F.; Li, W.; Yang, J.; Han, G.; Liao, P.; Sun, Y. Interfacing Nickel Nitride and Nickel Boosts Both Electrocatalytic Hydrogen Evolution and Oxidation Reactions. *Nat. Commun.* **2018**, *9*, 4531. [[CrossRef](#)]
36. Wang, H.; Liu, H.; Feng, T.; Wang, L.; Yuan, W.; Huang, Q.; Guo, Y. Electronically Modulated Nickel Boron by CeO_x Doping as a Highly Efficient Electrocatalyst towards Overall Water Splitting. *Dalton Trans.* **2022**, *51*, 675–684. [[CrossRef](#)]
37. Batugedara, T.N.; Brock, S.L. A Little Nickel Goes a Long Way: Ni Incorporation into Rh2P for Stable Bifunctional Electrocatalytic Water Splitting in Acidic Media. *ACS Mater. Au* **2023**, *3*, 299–309. [[CrossRef](#)]
38. Wang, Z.; Wang, H.; Ji, S.; Wang, X.; Zhou, P.; Huo, S.; Linkov, V.; Wang, R. A High Faraday Efficiency NiMoO_4 Nanosheet Array Catalyst by Adjusting the Hydrophilicity for Overall Water Splitting. *Chem. A Eur. J.* **2020**, *26*, 12067–12074. [[CrossRef](#)]
39. Elsharkawy, S.; Kutyla, D.; Marzec, M.M.; Zabinski, P. Electrodeposition of Hydrophobic Ni Thin Films from Different Baths under the Influence of the Magnetic Field as Electrocatalysts for Hydrogen Production. *Int. J. Hydrog. Energy* **2024**, *61*, 873–882. [[CrossRef](#)]
40. Sakamoto, Y.; Yuwasa, K.; Hirayama, K. X-Ray Investigation of the Absorption of Hydrogen by Several Palladium and Nickel Solid Solution Alloys. *J. Less Common. Met.* **1982**, *88*, 115–124. [[CrossRef](#)]
41. Elhamid, M.H.A.; Ateya, B.G.; Pickering, H.W. Effect of Benzotriazole on the Hydrogen Absorption by Iron. *J. Electrochem. Soc.* **1997**, *144*, L58–L61. [[CrossRef](#)]
42. Song, K.-D.; Kim, K.B.; Han, S.H.; Lee, H.K. A Study on Effect of Hydrogen Reduction Reaction on the Initial Stage of Ni Electrodeposition Using EQCM. *Electrochem. Commun.* **2003**, *5*, 460–466. [[CrossRef](#)]

43. Lioubashevski, O.; Katz, E.; Willner, I. Magnetic Field Effects on Electrochemical Processes: A Theoretical Hydrodynamic Model. *J. Phys. Chem. B* **2004**, *108*, 5778–5784. [[CrossRef](#)]
44. Aaboubi, O.; Chopart, J.P.; Douglade, J.; Olivier, A.; Gabrielli, C.; Tribollet, B. Magnetic Field Effects on Mass Transport. *J. Electrochem. Soc.* **1990**, *137*, 1796–1804. [[CrossRef](#)]
45. Budevski, E.; Staikov, G.; Lorenz, W.J. *Electrochemical Phase Formation and Growth: An Introduction to the Initial Stages of Metal Deposition*, 1st ed.; Wiley: Hoboken, NJ, USA, 1996; ISBN 978-3-527-29422-0.

Disclaimer/Publisher’s Note: The statements, opinions and data contained in all publications are solely those of the individual author(s) and contributor(s) and not of MDPI and/or the editor(s). MDPI and/or the editor(s) disclaim responsibility for any injury to people or property resulting from any ideas, methods, instructions or products referred to in the content.